Received: 30 October 2021 | Revised: 2 September 2022 | Accepted: 18 November 2022

IET Renewable Power Generation

DOI: 10.1049/rpg2.12665

The Institution of Engineering and Technology WILEY

ORIGINAL RESEARCH

An improved standalone photovoltaic system with hybrid dual integral sliding mode and model predictive control for MPPT

Neeraj Priyadarshi[1] | P. Sanjeevikumar[2] | M. S. Bhaskar[3] | Farooque Azam[4] | S. M. Muyeen[5]

[1]Department of Electrical Engineering, JIS College of Engineering, Kolkata, India

[2]Department of Electrical Engineering, IT and Cybernetic, University of South-Eastern Norway, Porsgrunn, Norway

[3]Renewable Energy Lab, College of Engineering, Prince Sultan University, Riyadh, Saudi Arabia

[4]School of Computer Science and Engineering, REVA University, Bangalore, India

[5]Department of Electrical Engineering, Qatar University, Doha, Qatar

Correspondence
S.M. Muyeen, Department of Electrical Engineering, Qatar University, Doha 2713, Qatar.
Email: sm.muyeen@qu.edu.qa

Abstract

In this research paper, a double diode model-based photovoltaic (PV) system with a proposed hybrid dual integral sliding mode control (DISMC) and model predictive control (MPC) based maximum power point tracker (MPPT) has been started for a standalone power system. Compared with the single diode model, the advanced model dual diode provides accurate maximum power point (MPP) estimation with high velocity and more searching efficiency. It also delivers the extrapolation of current-voltage characteristics of the photovoltaic system under any weather situation. Compared to classical sliding mode control (SMC) and dual integral sliding mode controller (DISMC) based MPPT, the proposed hybrid dual integral sliding mode controller (DISMC) and model predictive control (MPC) MPPT provide high, robust behavior with minimized steady-state error. A high gain multilevel boost converter is employed, which provides an output voltage directly proportional to the level number. Moreover, the predictive model controller extracts peak power from the PV module by predicting errors in further sampling periods and switching pulses. The proposed hybrid MPPT method provides a fixed switching frequency of a high gain multilevel boost converter under varying environmental and loading conditions. Practical responses justify the capability of advanced MPPT control using the dSPACEDS1104 platform.

1 | INTRODUCTION

Renewable energy sources are gaining more popularity compared to fossil fuels [1–3]. Among all renewable energy components, solar energy is treated as the cleanliest energy source [4–6]. The low conversion efficiency of photovoltaic (PV) systems is the major obstacle to renewable energy growth [7–9]. Comprehensive renovations have been introduced to enhance the photovoltaic tracking efficiency because of its non-linear behavior [10–12]. The MPPT techniques are the imperative inherent, which makes the system function optimally as the current and voltage characteristics of the PV cell have non-linear characteristics [13–15]. Hence, the maximum power point tracker (MPPT) is an essential component that ensures optimal power from PV modules [16–21]. Several MPPT algorithms have been implemented [22–25] in the past decades. The classical MPPT methods have been discussed, such as Perturb & Observe (P & O), constant current, incremental conductance, etc. Still, these methods cannot track global maximum power point (GMPP) under partial shade situations, antecedent deficient power conduction to load, and power destitution. Moreover, artificial intelligence algorithms, viz. Fuzzy logic control (FLC), Genetic algorithms (GA), artificial neural network (ANN) etc., have been implemented to conquer the detriment of classical MPPT methods. Large training data requirements, tuning of membership functions, and memory complexity are the major disadvantages that cannot track GMPP under partial shading conditions. Compared to the single diode approach of the PV system, the double diode model approach was introduced in this research work, which provides more accurate maximum power point evaluation and precise responses under complex computational situations.

In this research work, a model predictive controller (MPC) based double-diode integral sliding mode controller (DISMC)

is employed, which provides rapid response under varying environmental situations. This research work has discussed the proposed predictive controller by assuming lower switched frequency and higher rating power applications. The proposed MPC provides a prediction of controlling parameters under entire switched states. The major contribution of this manuscript is to enhance the behavior using the prediction of the error to get the desired controller parameters through MPC. The optimal switched state can be obtained by reducing the cost function. Moreover, a high gain multilevel boost converter is inserted in this research work compared to classical converters, which provide output voltage directly proportional to level numbers. In contrast to the boost switching capacitor converter, the proposed high gain boost multilevel converter provides high gain boost output voltage proportional to level number. The sliding mode controller (SMC) based MPPT provides flexible tracking control of non-linear DC-DC converters [26]. However, it comprehends complex filter construction because of inconstant conducting frequency and immense steady-state error. However, the proposed integral sliding mode controller yields minimized steady-state error, including the integral sliding area. This has also been noted that the performance of voltage control of high gain multilevel boost converter begun refined as one more integral expression has been supplemented to the controller sliding area, that is, double integral sliding mode controller (DISMC). Also, compared to classical sliding mode control (SMC), the proposed DISMC provides double integration to voltage tracked error, which reduces the steady-state error with compact, robust control. Pradhan et al. [26] have discussed DISMC based MPPT for standalone PV systems with a boost converter as an interface, under varying sun insolation. However, the performance of PV systems under partial shading situations has not been discussed in this manuscript. Rai et al. [27] have implemented a PV water pump design using ISMC, which is employed with rapid dynamics and sensorless operation for agricultural purposes. Fei et al. [28] investigated ISMC-based peak power tracking with high tracking action and low harmonic content. Khan et al. [29] demonstrated a neuro-based ITSMC for optimal PV power generation which provides robust performance, rapid converging speed, and fewer perturbations. Ali et al. [30] discussed an ST-ISMC controlled grid connected PV design which provides smooth capacitor voltage utilization, better regulation of DC-link voltage, and high power quality in changing environmental situations. Ayalew et al. [31] presented a CNMPC based ISMC for PV grid-tied systems that has better performance, robust behaviour, and fewer harmonics. Mousa et al. [32] and Ahmed et al. [33] presented SIMLBC with high gain transformation performance and used it for renewable applications. Moreover, the performance of SIMLBC has been equated with that of other classical topologies like MLBC, SIBC, etc. Radwan et al. [34] used FPGA to implement MLBC for PV with efficient optimal peak power achievement. Furthermore, in this research work, the proposed MLBC provides a high gain step up to a little voltage by using diodes and capacitor insertion.

The novelty of this manuscript is a double diode model-based PV approach with hybrid DISMC and SMC as the MPPT technique has been realized experimentally and analytically under different abnormal environmental conditions. It also provides superior performance in rapid loading conditions, and it is uncertain whether it is compared to DISMC based MPPT, discussed in Pradhan et al. [26]. The author's sincere observation is that this type of hybrid MPPT control system has neither been examined nor executed previously for a photovoltaic power system.

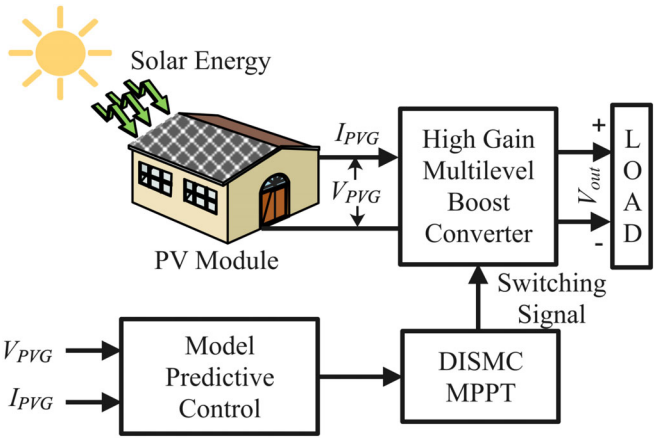

FIGURE 1 DISMC and MPC based PV system: Overall schematic structure

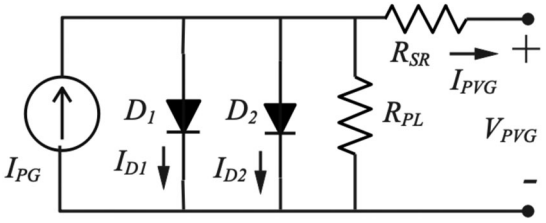

FIGURE 2 Double diode modeled PV cell

2 | HYBRID DISMC AND MPC BASED PV SYSTEM

Figure 1 depicts the advanced standalone PV structure in which a high gain multilevel boost converter works as a juncture between the PV module and the load. The hybrid DISMC and MPC-based methods act as an MPPT technique, producing a switching signal for the proposed converter.

2.1 | Double diode model based PV Cell

The employed double diode model provides extrapolation of *I-V* characteristics of a photovoltaic array under any operating conditions. Moreover, parameter estimation methodology can also be realized based on this double diode modeling. The current obtained from the equivalent circuit presented in Figure 2

is mathematically evaluated as [15, 16]:

$$I_{PVG} = I_{PG} - I_{RS1}\left[e^{\left(\frac{V_{PVG}+I_{PVG}R_{SR}}{A_{d1}V_{TR}}\right)-1}\right] - I_{RS2}\left[e^{\left(\frac{V_{PVG}+I_{PVG}R_{SR}}{A_{d2}V_{TR}}\right)-1}\right] - \left[\frac{V_{PVG}+I_{PVG}R_{SR}}{R_{PL}}\right], \quad (1)$$

where V_{PVG} is output voltage, I_{PG} is photo-generated current, R_{SR}, R_{PL} are shunt and series resistors, I_{RS1}, I_{RS2} are reverse saturation currents, A_{d1}, A_{d2} are ideality factors, and V_{TR} is thermal voltage and its value is calculated by,

$$V_{TR} = \frac{N_{SR}K_{Bol}T_{temp}}{Q_E}, \quad (2)$$

where N_{SR} is no. of series connected cells, K_{Bol} is Boltzmann constant, T_{temp} is temperature (K), and Q_E is electric charge. According to PN junction principle and silicon cell definition, the reverse saturation current of diffusion characteristics with temperature is evaluated as:

$$I_{RS1}(T_{temp}) = I_{RS1,ref}\left(\frac{T_{temp}}{T_{ref}}\right)^{\frac{3}{A_{d1}}} \times e^{\left[\frac{Q_E}{A_{d1}K_{Bol}}\left\{\frac{E_{gp}(T_{ref})}{Tref}\right\}-\left\{\frac{E_{gp}(T_{temp})}{Ttemp}\right\}\right]}, \quad (3)$$

where $I_{RS1,ref}$ is saturation current at reference environmental situation and T_{ref} is a temperature at reference environmental situations. Energy gap with time function is expressed mathematically as:

$$E_{gp}(T_{temp}) = E_{gp}(0) - \frac{AT_{temp}^2}{T_{temp}+B}. \quad (4)$$

Here, $E_{gp}(0)$ is reference energy at 0 K, and A and B are constants based on used materials. The R_{PL} and R_{SR} depends on irradiance (G) which is based on power function and temperature is based on linear function and expressed mathematically as:

$$R_{SR}(G, T_{temp}) = R_{SR,T_{temp}}\left[1 + K_{R_{SR}}(T_{temp} - T_{ref})\right] + R_{SR,G}\left(\frac{G}{G_{ref}}\right)^{-Y_{R_{SR}}R_{SR}}, \quad (5)$$

$$R_{PL}(G, T_{temp}) = R_{PL,ref}\left[1 - K_{R_{PL}}(T_{temp} - T_{ref})\right]\left(\frac{G}{G_{ref}}\right)^{-Y_{R_{PL}}R_{PL}}, \quad (6)$$

where $R_{SR,T_{temp}}$ is Dominant resistances for reference surrounding situations, $Y_{R_{SR}}$ and $Y_{R_{PL}}$ are Exponential coefficients of R_{SR} and R_{PL} w.r.t T_{temp}, respectively. $K_{R_{SR}}$ and $K_{R_{PL}}$ Linear coefficients of R_{SR} and R_{PL} w.r.t T_{temp}, respectively. Generated photocurrent increases with proportional increase of G as well as linear dependence on T_{temp} and mathematically expressed as:

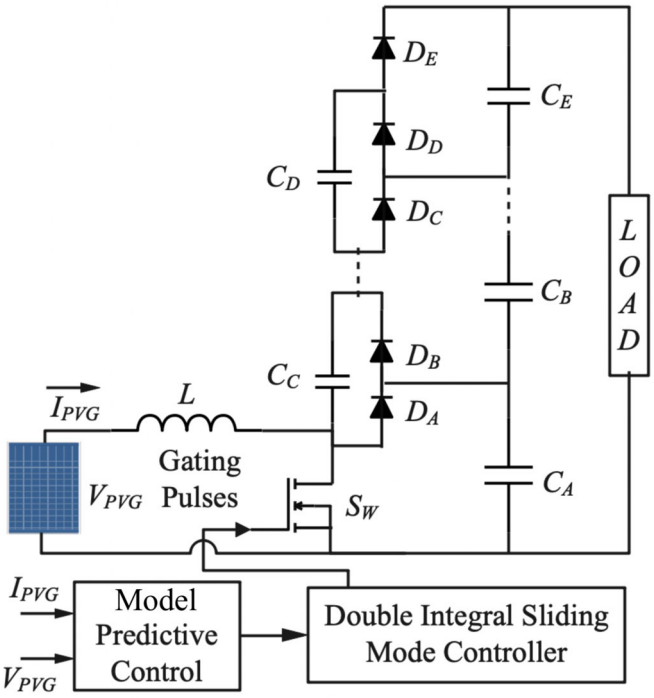

FIGURE 3 Multilevel boost converter (3-levels)

$$I_{PG}(G, T_{temp}) = \left[I_{PG,ref} + \alpha I_{short}(T_{temp} - T_{ref})\right]\left(\frac{G}{G_{ref}}\right). \quad (7)$$

Here, $I_{PG,ref}$ is generated photocurrent at reference surrounding situation, αI_{short} is linear coefficient of I_{short} w.r.t T_{temp}. Also, open circuit voltage dependency on environmental situations is expressed mathematically as:

$$V_{open}(G, T_{temp}) = V_{open,ref} + \beta V_{open}(T_{temp} - T_{ref}) + KV_{open}T_{temp}\log\left(\frac{G}{G_{ref}}\right), \quad (8)$$

where $V_{open,ref}$ is open circuit voltage at reference surrounding situation and βV_{open} and KV_{open} are coefficient of open circuit voltage w.r.t T_{temp} and G, respectively.

3 | MODELING OF MULTILEVEL BOOST CONVERTER

In this research work, a recent multilevel Boost converter topology (Figure 3) can be used to provide output voltage directly proportional to level numbers and be enhanced by summing two extra capacitors and diodes. Here, 2 level multilevel boost converter is employed for maximum power point tracking. The proposed converter operates when the switch is "ON" and "OFF" modes of operation[32–34]

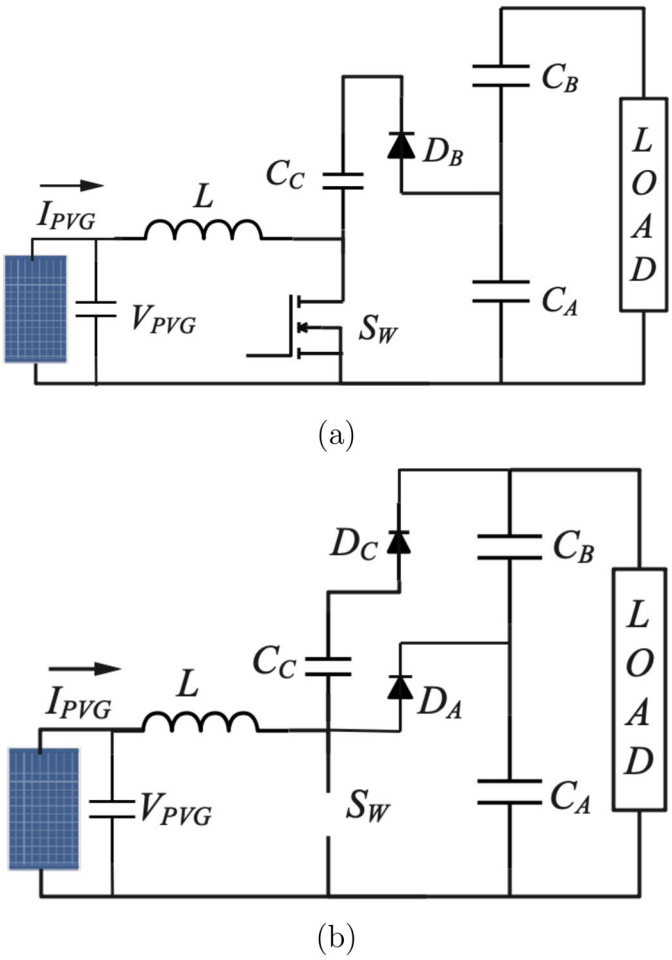

FIGURE 4 2-level boost converter. (a) *Mode I*: when switch is turned ON, (b) *Mode II*: when switch is turned OFF

Mode I: In mode I operation (Figure 4a), when the switch is "ON", the inductor starts conducting and capacitor C_A makes the capacitor C_C charged using diode D_B. It is also noted that $V_{C_C} < V_{C_A}$. Moreover, capacitors C_A and C_B provides the loading.

$$L_A \frac{dI_A}{dt} = V_{PVG} - I_{L_A} R_{L_A} - R_{ON-switch} \times \left[I_{L_A} + C_C \frac{dV_{C_C}}{dt} \right], \tag{9}$$

$$C_A \frac{dV_{C_A}}{dt} = \frac{-V_{C_A} + V_D + V_{C_C}}{R_{C_A}} + C_C \frac{dV_{C_C}}{dt} + \frac{R_{ON-switch}}{R_{C_A}} \left[I_{L_A} + C_C \frac{dV_{C_C}}{dt} \right]. \tag{10}$$

$$C_B \frac{dV_{C_B}}{dt} = \frac{-V_{C_B}}{R_{C_B}} + C_C \frac{dV_{C_C}}{dt}, \tag{11}$$

$$C_C \frac{dV_{C_C}}{dt} = \frac{\begin{bmatrix} V_{C_C} + V_D - V_{C_C} \\ + I_{L_A} R_{ON-switch} - I_{out} R_{C_A} \end{bmatrix}}{2R_{C_C} + R_{ON-switch}}. \tag{12}$$

Mode II: When the switch is OFF (Figure 4b), when switch is closed, diode D_A start working and inductor gets charged the capacitor C_A until its voltage is equivalent to addition of voltages across PV generator. Moreover, diode D_3 starts conducting and C_A and C_B gets charged, and voltage across the capacitors C_A and C_B becomes equivalent to addition of voltages across PV generator, C_C capacitor and voltage across inductor. The mathematical operation of voltage across inductor and current through the capacitor is expressed as:

$$L_A \frac{dI_A}{dt} = V_{PVG} - I_{L_A} R_{L_A} - V_{D_P} - R_{C_A} C_A \frac{dV_{C_A}}{dt}, \tag{13}$$

$$C_A \frac{dV_{C_A}}{dt} = I_{L_A} - I_{out} R_{L_A}, \tag{14}$$

$$C_B \frac{dV_{C_B}}{dt} = \frac{V_{C_C} - V_{C_A}}{R_{C_B}} + C_C \frac{dV_{C_C}}{dt}, \tag{15}$$

$$C_C \frac{dV_{C_C}}{dt} = \frac{V_{C_B} - V_{C_C}}{2R_{C_C}} - \frac{I_{out}}{2}. \tag{16}$$

It is also noted that, for subinterval one, V_{L_A} becomes the same as dc supply voltage. Under steady-state conditions, the entire volt-sec employed around one switched period should be 0 and negative. Theorem should be followed for the second

subinterval, and it should be negative for the second subinterval. Mathematically, Volt/s and charge balancing theorem for inductor and capacitor around one switched time can be expressed as:

$$L_A\frac{dI_A}{dt} = V_{Input} - I_L A_K + V_D\left[\frac{R_{switch}(2D_d-1)+R_{C_A}(1-D_d)}{2R_{C_A}+R_{switch}}\right] - R_{switch}D_d\left[\frac{V_{C_A}-V_{C_D}-I_{out}R_{C_A}}{2R_{C_A}+R_{switch}}\right] - V_{C_A}(1-D_d)+I_{out}R_{C_C}, \quad (17)$$

where $A_K = R_{L_A} + \frac{2R_{C_A}R_{switch}}{2R_{C_A}+R_{switch}} + R_{C_A}(1-D_d)$

$$C_A\frac{dV_{C_A}}{dt} = \frac{V_{VPG}}{(1-D_d)} - I_{out}\left[\frac{2R_{C_A}}{(1-D_d)} + \frac{2R_{L_A}}{(1-D_d)^2} + P_1 + Q_1(U_1+V_1)\right], \quad (18)$$

where

$$P_1 = \frac{8R_{swtch}^2R_{C_A}D_d}{(1-D_d)^2\left(2R_{C_A}+R_{switch}\right)}$$

$$Q_1 = \frac{D_dR_{switch}}{D_d(1-D_d)^2\left(2R_{C_A}+R_{switch}\right)}$$

$$U_1 = R_{switch}(1+2D_d)$$

$$V_1 = R_{C_A}(3(1-D_d)-D_d)-1$$

$$C_B\frac{dV_B}{dt} = \frac{V_{PVG}}{1-D_d} - V_d\left[\frac{R_{C_A}(3+D_d)}{1-D_d} + \frac{2R_{L_A}}{(1-D_d)^2} + P_2 + Q_2(V_2-U_2)\right], \quad (19)$$

where

$$P_2 = \frac{4R_{swtch}R_{C_A}D_d}{(1-D_d)^2\left(2R_{C_A}+R_{switch}\right)}$$

$$Q_2 = \frac{2R_{C_A}(1-D_d)+R_{switch}}{\left(2R_{C_A}+R_{switch}\right)}$$

$$U_2 = \frac{R_{switch}+(2-D_d)R_{C_A}}{D_d(1-D_d)}$$

$$V_2 = \frac{4(1-D_d)R_{C_A}+2(1-D_d)R_{switch}}{D_d(1-D_d)^2},$$

where C_A is capacitor value, R_{C_A} is capacitor's DC parasitic resistance, R_{switch} is ON switch resistance, V_D is the diode forward voltage, and R_{L_A} is Inductor's DC resistance. The capacitor charge balancing method is employed to evaluate the DC component of the current through the inductor. For the first subinterval, the capacitor provides a loading current that gets partial discharged. For the second subinterval, the current through the inductor provides loading and recharges the capacitor. Mathematically, the output voltage is derived as:

$$V_{out} = V_{C_A} + V_{C_B} = \frac{2V_{PVG}}{1-D_d} - V_d - I_{out}\left[\frac{R_{C_A}(5+D_d)}{1-D_d} + \frac{4R_{L_A}}{(1-D_d)^2} + W\right], \quad (20)$$

where $W = (P_1+P_2) + Q_1(U_1+V_1) + Q_2(U_2-V_2)$.

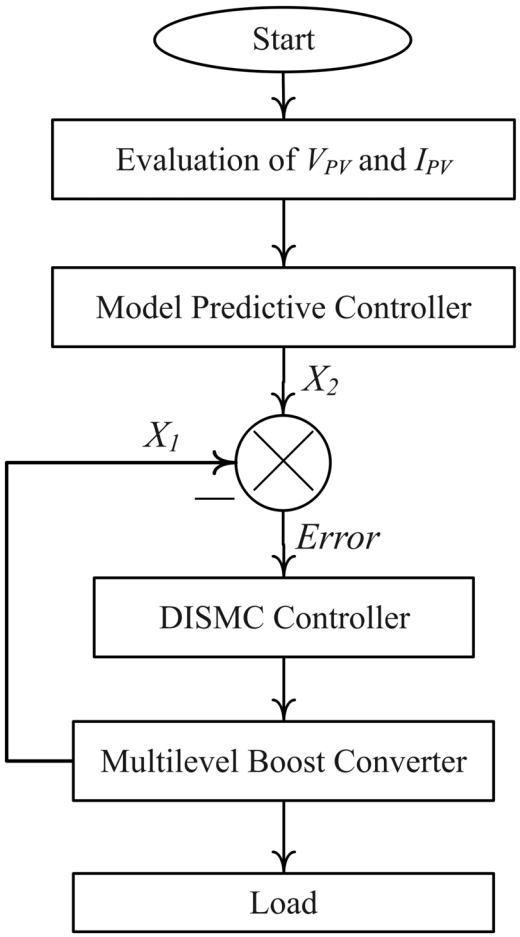

FIGURE 5 Flow chart of control system

4 | MODEL PREDICTIVE CONTROLLER

The flowchart for the control system has been presented using Figure 5 which clarifies the flow and connection of different parts of the MPC and DISMC controller. It comprises the essential constituents of MPC, DISMC, and a multilevel boost converter for the entire control system design. The MPC

accomplished prediction of controlling parameters under overall switched states and are able to speed up the performance by error prediction to achieve desired controlled parameters. Also, the multilevel boost converter delivers output voltage directly proportional to level numbers. And then DISMC provides double integration for voltage tracking error with reduced steady state error and robust control.

The model predictive controller-based MPPT provides fast-tracked behavior, accurate responses, and minimized settling period because of its predictive characteristics. The implication of MPC is important for high switching power applications, which predict the next performance of required controlling parameters till a predetermined horizon period. The MPC method predicts errors for the upcoming sample period by applying the cost function optimization method, and control action can be done by discrete expressions. Compared to other conventional MPPT controllers, MPC delivers sensor-less control with reduced cost, reliable operation, more straightforward implementation, and higher tracking efficiency as significant merits. This method predicts future behavior and errors in a single-stage coming to the horizon period by selecting a suitable actuating signal. Moreover, the required costing function has been reduced by selecting the actuating signal for the following predicting stages, which provides the prediction system nature of the upcoming sample period [35].

The future nature of required controller parameters can be predicted using the model predictive controller. It is employed to evaluate the optimal switched behavior. PV voltage and current act as input to this controller. With the evaluation of discrete-time variables from former sets of the equation. The nature of the controller may be decided for K_S sampling period. Mathematically, the converter's discrete-time modeling can be employed under switch ON condition, and predicted controller parameters could be derived as [36]:

$$I_{L_A}(K_S+1) = I_{L_A}(K_S)\left[1-\frac{R_{L_A}T_S'}{L_A}\right] + \frac{V_{PVG}(K_S)T_S'}{L_A}, \tag{21}$$

$$V_{PVG}(K_S+1) = V_{PVG}(K_S) \times \left[I_{PVG}(K_S)-I_{L_A}(K_S)\right]\frac{T_S'}{C_A}. \tag{22}$$

Under switch OFF Condition:

$$I_{L_A}(K_S+1) = I_{L_A}(K_S)\left[1-\frac{R_{L_A}T_S'}{L_A}\right] + \frac{V_{PVG}(K_S)T_S'}{L_A} - V_{C_A}(K_S), \tag{23}$$

$$V_{PVG}(K_S+1) = V_{PVG}(K_S) \times \left[I_{PVG}(K_S)-I_{L_A}(K_S)\right]\frac{T_S'}{C_A}. \tag{24}$$

Also, the derived mathematical expressions can be modeled using matrix form as:

$$\begin{bmatrix} I_{L_A}(K_S+1) \\ V_{PVG}(K_S+1) \end{bmatrix} = \begin{bmatrix} 1-R_{L_A}\frac{T_S'}{L_A} & \frac{T_S'}{L_A} \\ 0 & 2 \end{bmatrix}\begin{bmatrix} I_{L_A}(K_S) \\ V_{PVG}(K_S) \end{bmatrix} + \begin{bmatrix} 0 \\ -1 \end{bmatrix}\left[V_{PVG}(K_S-1)\right], \tag{25}$$

$$\begin{bmatrix} I_{L_A}(K_S+1) \\ V_{PVG}(K_S+1) \end{bmatrix} = \begin{bmatrix} 1 & 0 \\ 0 & 2 \end{bmatrix}\begin{bmatrix} I_{L_A}(K_S) \\ V_{PVG}(K_S) \end{bmatrix}. \tag{26}$$

The maximum power point tracker works because the slope of the PV characteristics curve becomes zero on the maximum point region, +ve (positive) on the left, and −ve (negative) towards the right of the predicted maximum power point region. The output of the predictive controller acts as input to the double integral sliding mode controller.

5 | DUAL INTEGRAL SLIDING MODE CONTROLLER

The DISMC may be designed for proper adjustment of current through the inductor, photovoltaic current I_{PVG} and voltage V_{PVG} such that maximum extraction of PV power. The proposed MPPT algorithm evaluates reference voltage V_{Ref} to calculate maximum power point tracking. The reference voltage can be evaluated using the mathematical relation, $V_{Ref} = K_{open}V_{open}$; where, K_{open} is a coefficient of the material of the PV array. The double integral sliding mode can be designed as:

Step I: The required duty cycle of multilevel boost converter can estimate as:

$$\%\delta_{duty} = \frac{V_{out}-V_{PVG}}{V_{out}} \times 100, \tag{27}$$

$$\%\delta_{Ref} = \frac{V_{out}-V_{Ref}}{V_{out}} \times 100. \tag{28}$$

Step II: Selection of switched area $S_S(X_S)$, where X_S State notation and can be expressed mathematically as:

$$S_S(X_S) = \left[\frac{d}{dt}+\alpha\right]^{N-1} E_S(X_S), \tag{29}$$

where N is degree of sliding area, $E_S(X_S)$ is tracked error. If N=1, then $S_S(X_S) = E_S(X_S)$. Also, the tracking error E can be expressed as:

$$E_S(X_S) = E_S(X_{S_1}) + E_S(X_{S_2}) + E_S(X_{S_3}), \tag{30}$$

where,

$$\begin{cases} E_S(X_{S_1}) = \left(V_{Ref}-V_{PVG}\right) \\ E_S(X_{S_2}) = \int \left(V_{Ref}-V_{PVG}\right)dT_P \\ E_S(X_{S_3}) = \int\left\{\int \left(V_{Ref}-V_{PVG}\right)dT_P\right\}dT_p \end{cases}. \tag{31}$$

Step III: To apply invariance principle for evaluating equivalent control (U_{EQ}^{E}):

$$S_S(X_S) = \dot{S}_S(X_S), \text{then } U_r^E \cong U_{EQ}^E. \tag{32}$$

It is also noted that (U_{EQ}) (Equivalent controller) provides workable sliding movement on the switched surface.

$$S_S(X_S) = 0; \dot{S}_S(X_S) = 0. \tag{33}$$

By solving ((33)), we get,

$$U_{EQ}^E = -\hat{G}^{-1}\left[\hat{F}_S E_S\left(X_{S_1}\right) + E_S\left(X_{S_2}\right)\right] = \hat{G}^{-1}\hat{U}_r^E, \tag{34}$$

$$\hat{U}_r^E = -\left[\hat{F}_S E_S\left(X_{S_1}\right) + E_S\left(X_{S_2}\right)\right]. \tag{35}$$

Step IV: Applying Lyapunov's stability criteria:

$$S_S(X_S)\dot{S}_S(X_S) < 0. \tag{36}$$

Also, non-linear switched signal (u_m) is responsible for external perturbations and expressed as:

$$\left\{ u_m = -\hat{G}^{-1}K_t|S_S(X_S)|^{\beta} sat\left(\frac{S_S(X_S)}{\phi_{TM}}\right), \quad 0 < \beta < 1, \right. \tag{37}$$

$$sat\left(\frac{S_S(X_S)}{\phi_{TM}}\right) = \begin{cases} 1 & \left|\frac{S_S(X_S)}{\phi_{TM}}\right| \le 1 \\ signum\left(\frac{S_S(X_S)}{\phi_{TM}}\right) & \left|\frac{S_S(X_S)}{\phi_{TM}}\right| > 1 \end{cases}, \tag{38}$$

The component $|S_S(X_S)|^{\beta}$ emphasizes u_m that reached velocity enhances only when the state is far from the sliding area. Moreover, reached velocity decreases nearer to sliding areas. Chattered amplitude is decreased through interpolating u_m into the thinner boundary with ϕ_{TM} thickness. K_t should be larger such that reached situation $S_S(X_S)\dot{S}_S(X_S) < 0$ holds. K_t will be evaluated using the reachability method: $\frac{1}{2}\frac{d}{dt}S_S(X_S)^2 \le -\eta_t|S_S(X_S)|$. Reached period is estimated as:

$$T_{Rch} \le \frac{S_S(X_S)(T_R = 0)}{\eta_t}. \tag{39}$$

Also, K_t can be evaluated as:

$$K_t \ge \hat{G}_S\hat{G}_S^{-1}(\hat{F}_S - F_t) + \hat{F}_S + \hat{G}_S\hat{G}_S^{-1}(E_S(X_{S_1}) + E_S(X_{S_2})). \tag{40}$$

Step V: Switched controlled signal can be estimated as:

$$\begin{aligned} U_r^E &= U_{EQ}^E + u_m \\ &= G_S^{-1}\left[\hat{U}_r^E - K_t|S_S(X_S)|^{\beta} sat\left(\frac{S_S(X_S)}{\phi_{TM}}\right)\right]. \end{aligned} \tag{41}$$

Step VI: Percentage of duty ratio (δ_{duty}) can be evaluated using loading voltage and PV generated voltage.

Step VII: For checking sliding mode convergence, Lyapunov function $V_L(X_S)$ can be employed as: $V_L(X_S) = \frac{1}{2}S_S^T(X_S)S_S(X_S)$. For ensuring present situation, $\dot{V}_L(X_S)$ should be less than 0, such that,

$$\dot{V}_L(X_S) = \dot{S}_S(X_S)S_S(X_S) = S_S(X_S)\{F_S(X_S)\} < 0. \tag{42}$$

Moreover, for proposed photovoltaic system:

$$\begin{aligned} \dot{S}_S(X_S) &= \frac{d}{dt}\left[E_S\left(X_{S_1}\right) + E_S\left(X_{S_2}\right) + E_S\left(X_{S_3}\right)\right] \\ &= \dot{V}_{PVG}[1 + V^*] = \left[\frac{I_{L_A}}{C_A} - \frac{V_{PVG}}{C_A R_{PVG}}\right][1 + V^*] \\ &\cong \left[\frac{I_{L_A}}{C_A} - \frac{V_{PVG}}{C_A R_{PVG}}\right][V^*] = -B_1 B_2, \end{aligned} \tag{43}$$

where $V^* = V_{Ref} - V_{PVG} + \int(V_{Ref} - V_{PVG})dT_P$. In this case, $R_{PVG} < 0$; therefore, the component $(\frac{-V_{PVG}}{C_A R_{PVG}}) > 0$. Hence, $\dot{S}_S(X_S)$ sign is dependent of B_2 sign. Therefore, If $S_S(X_S) > 0$, $B_2 > 0$, then $\dot{S}_S(X_S) < 0$ and if $S_S(X_S) < 0$, $B_2 < 0$, then $\dot{S}_S(X_S) > 0$. Moreover, chattering amplitude H_A is evaluated as: $H_A = H_{A_1} - H_{A_2}$; where H_{A_1} and H_{A_2} are the highest and lowest chattering point, respectively, of PV signal.

$$SSE = \left|V_{Ref} - \left[H_{A_2} + \frac{H_{A_1} - H_{A_2}}{2}\right]\right|. \tag{44}$$

6 | RESULTS AND DISCUSSION

Simulation responses have been depicted to estimate the high performance of advanced MPPT algorithms under changing atmospheric situations. The performance of the proposed MPPT method is compared with DISMC based MPPT. Figure 6 presents the simulated responses under varying solar insolation while the temperature is kept fixed. The proposed MPPT method has high PV power tracking capability and negligible oscillations nearer to MPP locations than DISMC method-based MPPT. Figure 7 demonstrates the simulated result under changing temperature while the solar insolation level is kept fixed. The proposed MPPT algorithm has optimal PV power tracking performance and less oscillation around the MPP region. The practical responses are justified by conducting experimentation using the dSPACE DS1104 platform under varying environmental conditions. Major components are PV module, high gain multilevel boost converter, signal conditioner, filter circuits, and dSPACE kit, which are depicted in Figure 8. Experimental responses presented in Figure 9 (left) depict the proposed MPPT algorithm provides optimal PV power tracking with zero oscillation nearer to MPP locations in equated with Perturb and Observe and DISMC based MPPT under changing environmental conditions.

Figure 9 (right) presents the generated duty ratio of high gain multilevel boost converter under partial shade conditions using perturb and observe MPPT, DISMC MPPT, and proposed MPPT. Figure 9 provides better voltage regulation of

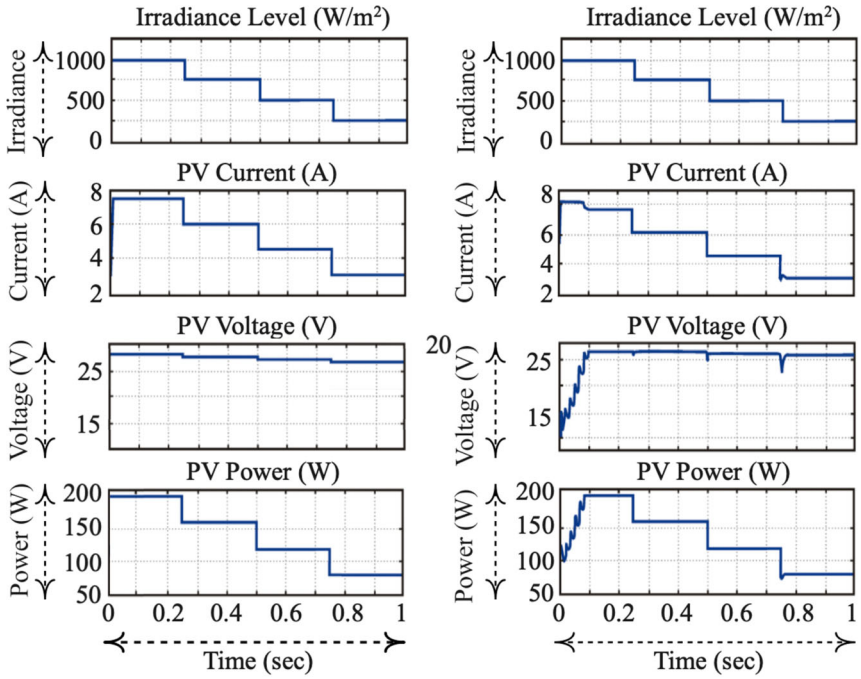

FIGURE 6 Simulation results under changing sun insolation with proposed control (left) and conventional DISMC MPPT (right)

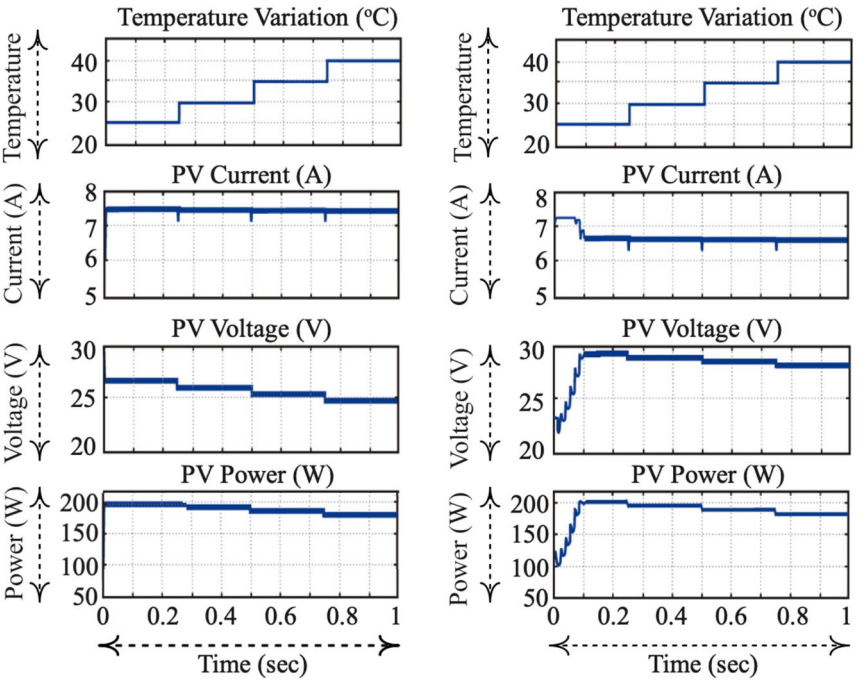

FIGURE 7 Simulation results under changing temperature condition with proposed control (left) and conventional DISMC MPPT (right)

high gain multilevel boost converter compared to employed DISMC and perturb and observe methods of MPPT. The performance of the proposed hybrid DISMC-MPC based PV system has been evaluated under varying sun insolation 1000 W/m^2 to 700 W/m^2 and then vice versa. Practical results presented in Figure 10 depict the superior PV tracking performance with the lowest MPP tracking period. Figure 11 presents the performance comparison of proposed hybrid DISMC – MPC based MPPT with incremental conductance (INC) and perturb and observe (P & O) based MPPT under varying solar irradiance, respectively. The proposed hybrid DISMC –MPC-based MPPT provides superior PV power tracking capability equated with INC and P & O based MPPT. Figure 12 depicts the obtained functional *I-V* characteristics of the PV module using the employment of an advanced modeled double diode and proposed hybrid DISMC-MPC based MPPT. This provides accurate maximum power point (MPP) estimation with high velocity and more searching efficiency and the

FIGURE 8 Practical setup of proposed PV system

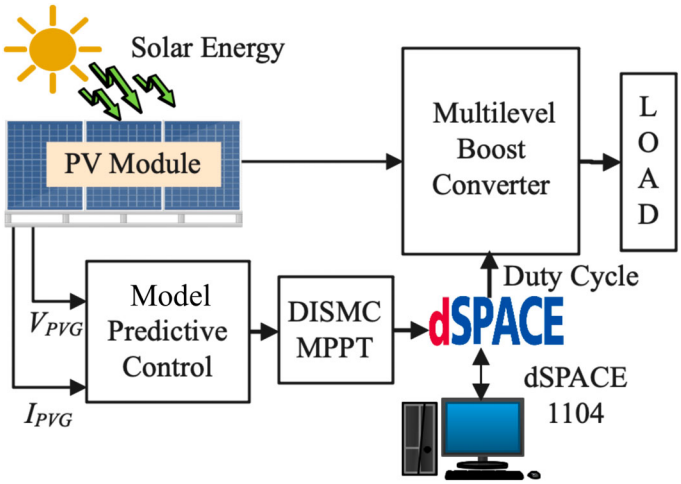

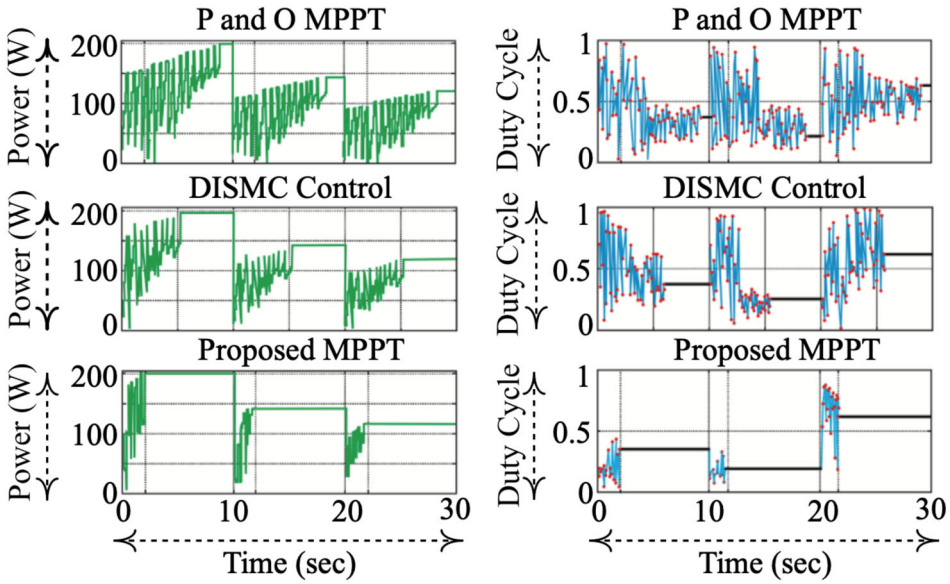

FIGURE 9 Experimental results under changing environmental condition: PV power tracking (left) and duty ratio of high gain multilevel boost converter (right)

extrapolation of current-voltage characteristics of the photovoltaic system under any weather situations. Figure 13 presents the practically obtained accurate P-V characteristics under varying sun insolation and ambient temperature, respectively. Figure 14 demonstrates the performance of standalone PV system under changing atmospheric condition using proposed DISMC-MPC and DISMC based MPPT controllers, respectively. This reveals that the proposed DISMC-MPC based MPPT delivers fast, accurate, and lowest oscillation around the MPP region compared to DISMC based MPPT [26]. The observed behavior of the proposed hybrid DISMC-MPC based MPPT has been evaluated under fixed environmental conditions (G=750 W/m^2 and $T = 500C$). In contrast, resistive loading conditions are varied from 5Ω to 50Ω. Figure 15 presents the experimental results found under conditions as mentioned earlier with high accuracy and optimal PV power tracking. The efficiency vs. PV power output plot has been obtained practically in Figure 16 for the proposed hybrid DISMC-MPC vs. conventional DISMC based MPPT controller. Under changing solar irradiance, which reveals the PV system's superior PV power tracking capability using proposed hybrid DISMC-MPC MPPT. Tables 1, 2 , 3 and 4 present the DISMC-MPC parameters employed during experimentation, 200 W PV panel specifications, multilevel boost converter parameters and quantitative comparison of MPPT employed methods, respectively. Figure 17 demonstrates the bode notation of the employed photovoltaic system under $G = 1200$ W/m^2 and 50 W/m^2. The presented bode plot reveals that the employed photovoltaic system has been found stable for both solar insolations. Hence, the proposed hybrid model predictive DISMC

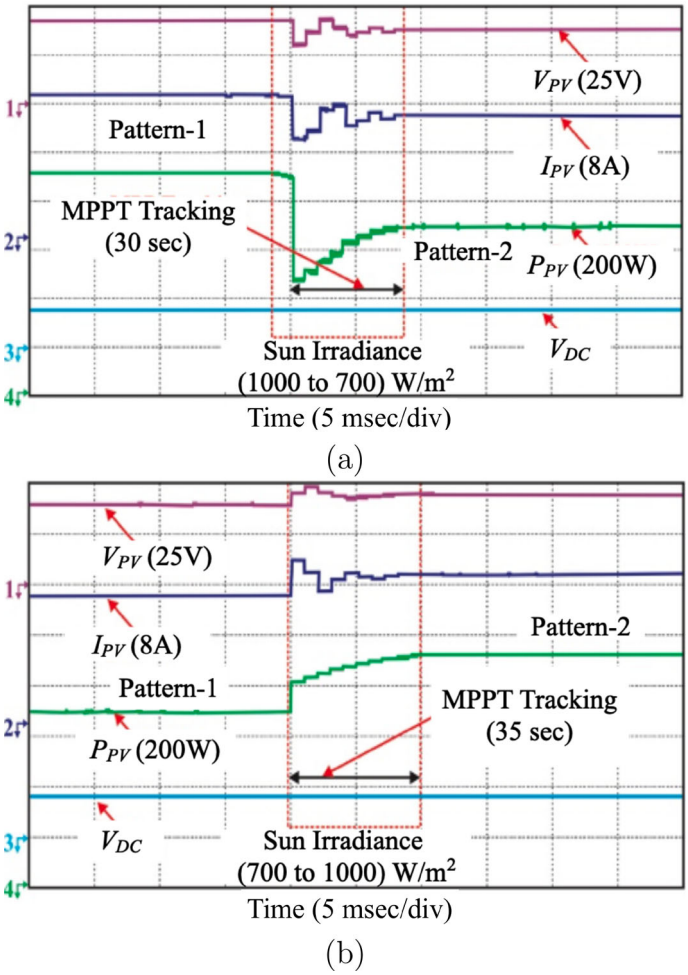

FIGURE 10 Practical results of behavior of proposed controller under (a) decreasing sun insolation; (b) increasing sun insolation

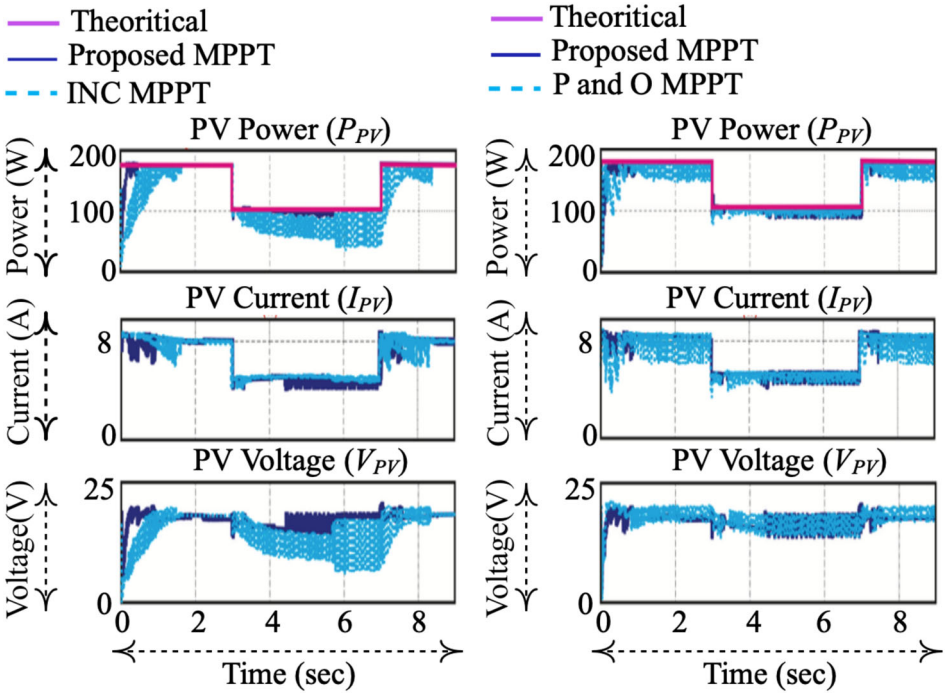

FIGURE 11 Practical compared results of behavior of proposed hybrid DISMC-MPC MPPT controller with INC MPPT (left), and P and O MPPT (right) under varying sun insolation

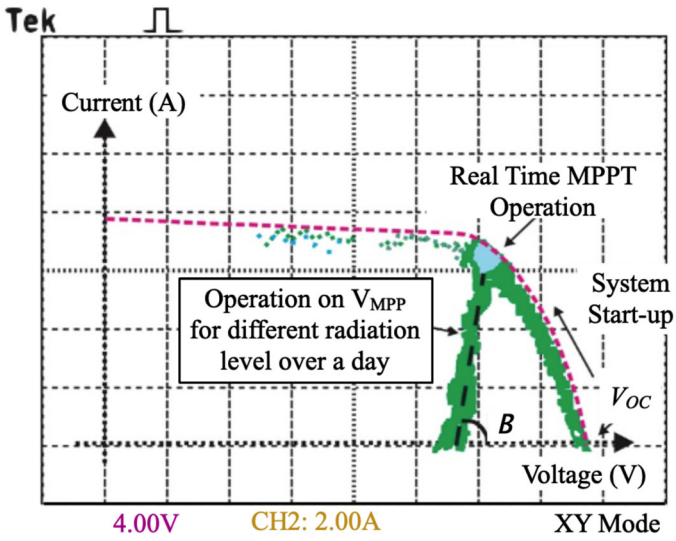

FIGURE 12 Practical *I–V* characteristics obtained

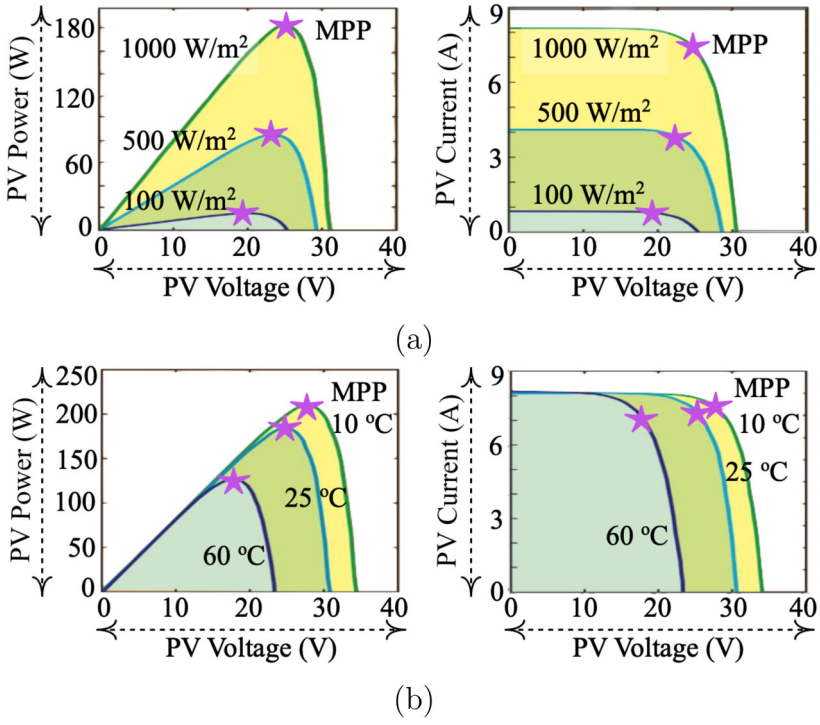

FIGURE 13 Practical *P-V* characteristics under (a) varying sun insolation (b) varying temperature

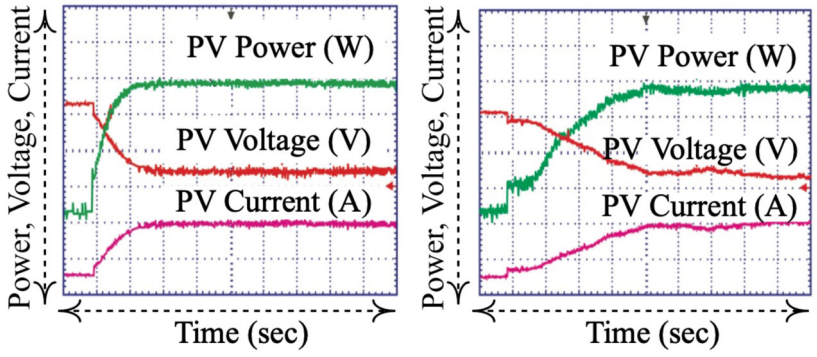

FIGURE 14 Practical results of behavior of PV system under changing atmospheric condition (Power=200 W, Voltage = 25 V, Current = 8 A) with proposed MPPT (left) and DISMC MPPT (right)

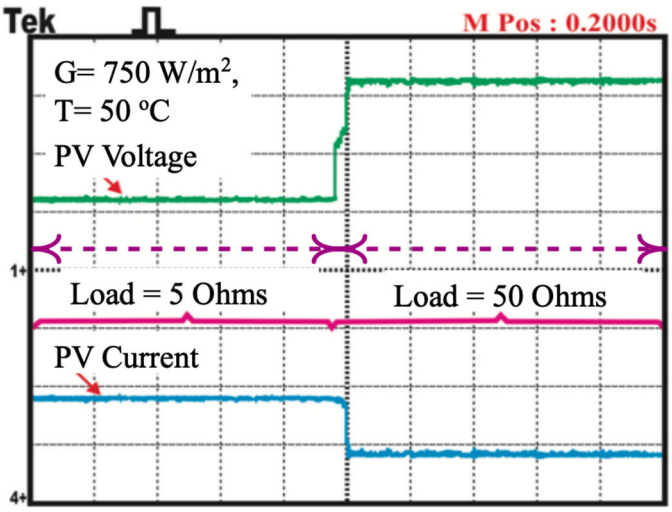

FIGURE 15 Practical results of behavior of PV system with proposed hybrid DISMC-MPC based MPPT under varying load condition

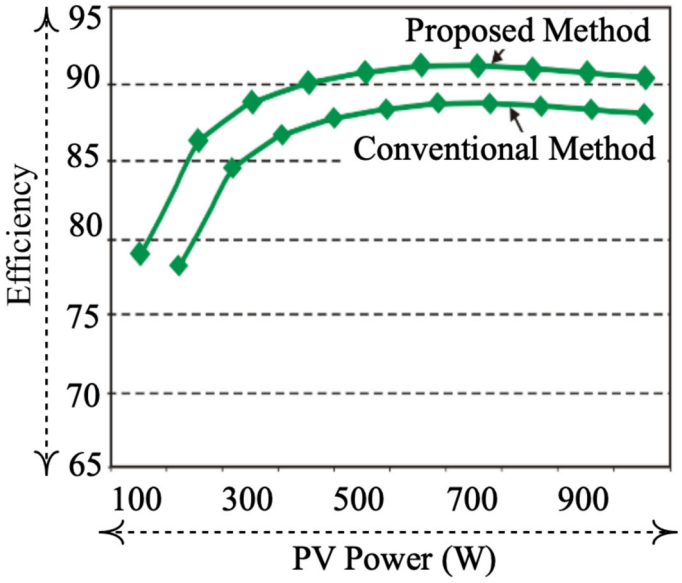

FIGURE 16 Practical results of efficiency versus power for proposed controller and conventional DISMC MPPT under varying sun insolation

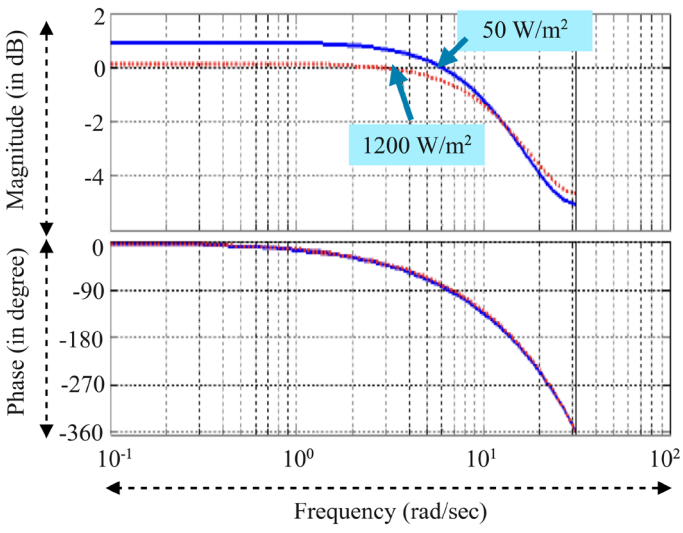

FIGURE 17 Bode plot which verify the robustness of system

TABLE 1 DISMC-MPC parameters employed during experimentation

Parameters	Values
Amplitude of PV voltage fluctuations H_A	0.005
Steady state error (%)	0.0015
Settling period (s)	0.10

TABLE 2 200 W PV panel specification

Parameters	Values
P^{max} (Peak power)	200 W
V^{max} (Peak voltage)	26.6 V
I^{max} (Peak current)	7.52 A
V_{OC} (Open circuited voltage)	33.2 V
I_{SC} (Short circuited current)	8.36 A

TABLE 3 Multilevel boost converter specifications

Parameters	Values
Inductor L_A	1.50 mH
Capacitor $C_A = C_B = C_C$	25 μF
R_{load}	100 Ω
Switching frequency	20 kHz

based controller provides stable operation for a large domain of solar irradiance. The performance of photovoltaic systems has been evaluated under step changes, which prove MPPT operation using SMC, DISMC, and proposed DISMC-MPC methods. Using the proposed DISMC-MPC method, the PV system has high tracked velocity, reliable operation, lower steady state error, negligible steady state oscillation, and higher efficacy with simpler implementation compared to SMC and DISMC as presented in Figure 18.

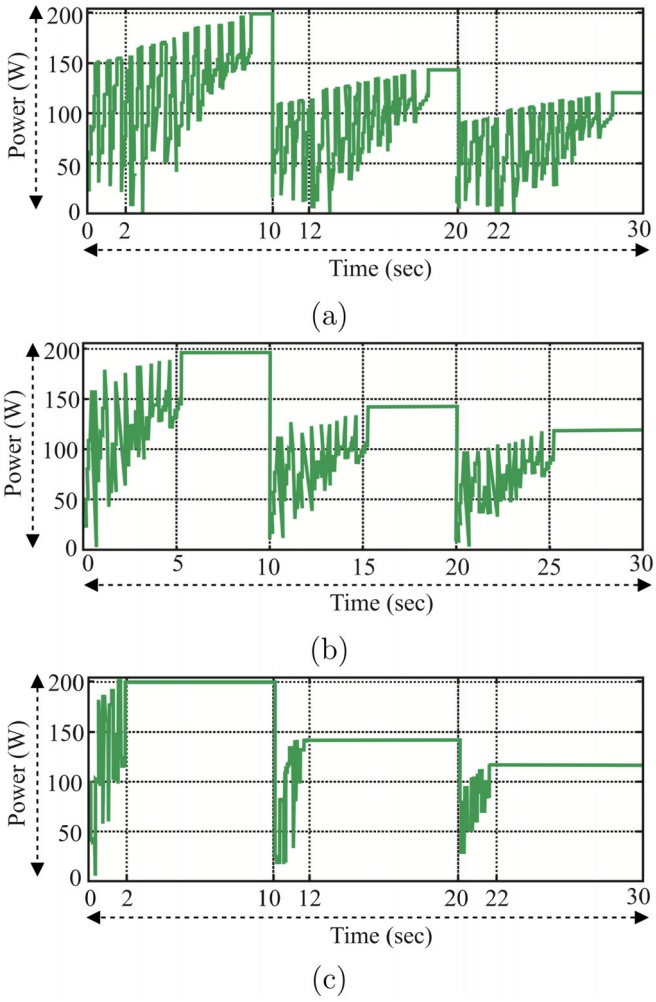

FIGURE 18 Practical found performance under step changes using (a) SMC, (b) DISMC and (c) DISMC-MPC

7 | CONCLUSION

This paper presented a double diode model-based PV system with a hybrid model predictive controller, and DISMC based MPPT has been employed for improved MPPT efficiency. The proposed double diode model-based PV system can deliver extrapolation of the photovoltaic system's P-V characteristics under any abnormal conditions. A high gain multilevel converter is used, which delivers output voltage directly proportional to level numbers. The predictive model controller provides error prediction for the coming sample period before the application of gating pulses. The proposed hybrid MPPT

TABLE 4 Quantitative comparison of MPPT methods

Parameters	P&O	INC	SMC	DISMC	Proposed (DISMC-MPC)
Simpler implementation	Easy	Easy	Moderate	Moderate	Moderate
Efficacy	Low	Low	High	High	Higher
Tracked velocity	Low	Low	Moderate	Moderate	High
Reliable	Low	Low	Moderate	High	Higher
Steady state error	High	High	Moderate	Low	Lower
Steady state oscillation	Yes	Yes	Moderate	Moderate	No

method accomplishes superior estimation of maximum power point online and high accuracy with utmost tracking efficiency. Practical validation of the proposed design has been justified experimental quantitative comparison has been validated for the proposed DISMC-MPC based PV system with SMC, DISMC, and DISMC-MPC methods. Furthermore, experimental justification is provided for the proposed hybrid DISMC-MPC based MPPT under varying loading and solar insolations using the dSPACE DS1104 platform.

AUTHOR CONTRIBUTIONS

Neeraj Priyadarshi: Conceptualization, data curation, formal analysis, investigation, methodology, project administration, software, writing - original draft. P. Sanjeevikumar: Methodology, supervision, validation, visualization, writing - review and editing. Mahajan Sagar Bhaskar: Methodology, project administration, software, supervision, validation, visualization, writing - review and editing. Farooque Azam: Investigation, methodology, validation, visualization, writing - review and editing. S. M. Muyeen: Funding acquisition, project administration, supervision, validation, writing - review and editing.

ACKNOWLEDGEMENT

The publication of this article was funded by Qatar National Library.

CONFLICT OF INTEREST

The authors have declared no conflict of interest.

DATA AVAILABILITY STATEMENT

Data sharing is not applicable - no new data is generated.

ORCID

Neeraj Priyadarshi https://orcid.org/0000-0001-6620-6771
P. Sanjeevikumar https://orcid.org/0000-0003-3212-2750
M. S. Bhaskar https://orcid.org/0000-0002-3147-2532
S. M. Muyeen https://orcid.org/0000-0003-4955-6889

REFERENCES

1. Prabhakaran, K., Karthikeyan, A., Varsha, S., Perumal, B.V., Mishra, S.: Standalone single stage pv-fed reduced switch inverter based pmsm for water pumping application. IEEE Trans. Ind. Appl. 56(6), 6526–6535 (2020)
2. Kumar, M., Tyagi, B.: A robust adaptive decentralized inverter voltage control approach for solar pv and storage based islanded microgrid. IEEE Trans. on Ind. Appl. 57(5), 5356–5371 (2021)
3. Shams, I., Mekhilef, S., Tey, K.S.: Improved-team-game-optimization-algorithm-based solar mppt with fast convergence speed and fast response to load variations. IEEE Trans. Ind. Electron. 68(8), 7093–7103 (2020)
4. Zhang, X., Gamage, D., Wang, B., Ukil, A.: Hybrid maximum power point tracking method based on iterative learning control and perturb & observe method. IEEE Trans. Sustain. Energy 12(1), 659–670 (2020)
5. Lin, B., Wang, L., Wu, Q.: Maximum power point scanning for pv systems under various partial shading conditions. IEEE Trans. Sustain. Energy 11(4), 2556–2566 (2020)
6. Raiker, G.A., Loganathan, U., Reddy B, S.: Current control of boost converter for pv interface with momentum based perturb and observe mppt. IEEE Trans. Ind. Appl. 57(4), 4071–4079 (2021)
7. Tang, C.-Y., Wu, H.-J., Liao, C.-Y., Wu, H.-H.: An optimal frequency-modulated hybrid mppt algorithm for the llc resonant converter in pv power applications. IEEE Trans. Power Electron. 37(1), 944–954 (2021)
8. Peng, Q., Tang, Z., Yang, Y., Liu, T., Blaabjerg, F.: Event-triggering virtual inertia control of pv systems with power reserve. IEEE Trans. Ind. Appl. 57(4), 4059–4070 (2021)
9. Shukla, S., Singh, B., Shaw, P., Al-Durra, A., El-Fouly, T.H., El-Saadany, E.F.: A new analytical mppt based induction motor drive for solar pv water pumping system with battery backup. IEEE Trans. Ind. Electron. 69(6), 5768–5781 (2021)
10. Jately, V., Bhattacharya, S., Azzopardi, B., de Montgareuil, A.G., Joshi, J., Arora, S.: Voltage and current reference based mppt under rapidly changing irradiance and load resistance. IEEE Trans. Energy Con. 36(3), 2297–2309 (2021)
11. Pervez, I., Shams, I., Mekhilef, S., Sarwar, A., Tariq, M., Alamri, B.: Most valuable player algorithm based maximum power point tracking for a partially shaded pv generation system. IEEE Trans. Sustainable Energy 12(4), 1876–1890 (2021)
12. Priyadarshi, N., Bhaskar, M.S., Padmanaban, S., Blaabjerg, F., Azam, F.: New cuk–sepic converter based photovoltaic power system with hybrid gsa–pso algorithm employing mppt for water pumping applications. IET Power Electron. 13(13), 2824–2830 (2020)
13. Priyadarshi, N., Padmanaban, S., Holm-Nielsen, J.B., Bhaskar, M.S., Azam, F.: Internet of things augmented a novel pso-employed modified zeta converter-based photovoltaic maximum power tracking system: hardware realisation. IET Power Electron. 13(13), 2775–2781 (2020)
14. Lin, D., Li, X., Ding, S., Wen, H., Du, Y., Xiao, W.: Self-tuning mppt scheme based on reinforcement learning and beta parameter in photovoltaic power systems. IEEE Trans. on Power Electron. 36(12), 13826–13838 (2021)
15. Priyadarshi, N., Padmanaban, S., Maroti, P.K., Sharma, A.: An extensive practical investigation of fpso-based mppt for grid integrated pv system under variable operating conditions with anti-islanding protection. IEEE Syst. J. 13(2), 1861–1871 (2018)
16. Priyadarshi, N., Padmanaban, S., Bhaskar, M.S., Blaabjerg, F., Sharma, A.: A fuzzy svpwm based inverter control realization of grid integrated pv-wind system with fpso mppt algorithm for a grid-connected pv/wind power generation system: Hardware implementation. IET Electric Power Appl. 12(7), 962–971 (2018)
17. Sen, A., Singh, B.: Peak current detection starting based position sensorless control of bldc motor drive for pv array fed irrigation pump. IEEE Trans. Ind. Appl. 57(3), 2569–2577 (2021)
18. Priyadarshi, N., Padmanaban, S., Holm-Nielsen, J.B., Blaabjerg, F., Bhaskar, M.S.: An experimental estimation of hybrid anfis–pso-based mppt for pv grid integration under fluctuating sun irradiance. IEEE Syst. J. 14(1), 1218–1229 (2019)
19. López-Erauskin, R., González, A., Petrone, G., Spagnuolo, G., Gyselinck, J.: Multi-variable perturb and observe algorithm for grid-tied pv systems with joint central and distributed mppt configuration. IEEE Trans. Sustain. Energy 12(1), 360–367 (2020)
20. Pindado, S., Roibás-Millán, E., Cubas, J., Álvarez, J.M., Alfonso-Corcuera, D., Cubero-Estalrrich, J.L., Gonzalez-Estrada, A., Sanabria-Pinzón, M., Jado-Puente, R.: Simplified lambert w-function math equations when applied to photovoltaic systems modeling. IEEE Trans. Ind. Appl. 57(2), 1779–1788 (2021)
21. Ostadrahimi, A., Mahmoud, Y.: Novel spline-mppt technique for photovoltaic systems under uniform irradiance and partial shading conditions. IEEE Trans. Sustain. Energy 12(1), 524–532 (2020)
22. Saxena, V., Kumar, N., Singh, B., Panigrahi, B.K.: A rapid circle centre-line concept-based mppt algorithm for solar photovoltaic energy conversion systems. IEEE Trans. Circuits Syst. I: Regular Papers 68(2), 940–949 (2020)
23. Figueiredo, S., e Silva, R.N.A.L.: Hybrid mppt technique pso-p&o applied to photovoltaic systems under uniform and partial shading conditions. IEEE Latin America Trans. 19(10), 1610–1617 (2021)
24. Sangwongwanich, A., Blaabjerg, F.: Mitigation of interharmonics in pv systems with maximum power point tracking modification. IEEE Trans. power Electronics 34(9), 8279–8282 (2019)

25. Chang, M.-C., Liu, S.-I.: An indoor photovoltaic energy harvester using time-based mppt and on-chip photovoltaic cell. IEEE Trans. Circuits Syst. II: Exp. Briefs 67(11), 2432–2436 (2020)
26. Pradhan, R., Subudhi, B.: Double integral sliding mode mppt control of a photovoltaic system. IEEE Trans. Control Syst. Tech. 24(1), 285–292 (2015)
27. Rai, R., Shukla, S., Singh, B.: Sensorless field oriented smcc based integral sliding mode for solar pv based induction motor drive for water pumping. IEEE Trans. Ind. Appl. 56(5), 5056–5064 (2020)
28. Fei, L., Jiandi, Z.: The mppt technology based on integral sliding mode control. In: 2017 IEEE Int. Conf. Inf. Autom. (ICIA), pp. 288–292. IEEE, Piscataway (2017)
29. Khan, Z.A., Khan, L., Khan, Q., Khan, U.H., Karam, F.W., Khan, M.A.: Neuro based integral terminal sliding mode nonlinear mppt control paradigms for stand-alone photovoltaic system. In: 2019 22nd International Multitopic Conference (INMIC), pp. 1–8. IEEE, Piscataway (2019)
30. Ali, M., Krama, A., Refaat, S.S.: A robust grid-tied pv system based super-twisting integral sliding mode control. In: 2021 10th International Conference on Renewable Energy Research and Application (ICRERA), pp. 402–407. IEEE, Piscataway (2021)
31. Ayalew, B., Yahaya, A.A., Al Durra, A.: Robust continuous nonlinear predictive controller (cnmpc) via integral sliding mode control (ismc) for grid-tied pv inverter. In: 2020 2nd International Conference on Smart Power & Internet Energy Systems (SPIES), pp. 514–519. IEEE, Piscataway (2020)
32. Mousa, M., Ahmed, M., Orabi, M.: A switched inductor multilevel boost converter. In: 2010 IEEE international conference on Power and Energy, pp. 819–823. IEEE, Piscataway (2010)
33. Ahmed, M.E., Mousa, M., Orabi, M.: Development of high gain and efficiency photovoltaic system using multilevel boost converter topology. In: The 2nd International Symposium on Power Electronics for Distributed Generation Systems, pp. 898–903. IEEE, Piscataway (2010)
34. Radwan, H., Mousa, M., Ahmed, M., Orabi, M.: Implementation of fpga control for multilevel boost converter used for pv applications. In: The 2nd International Symposium on Power Electronics for Distributed Generation Systems, pp. 70–75. IEEE, Piscataway (2010)
35. Metry, M., Shadmand, M.B., Balog, R.S., Abu-Rub, H.: Mppt of photovoltaic systems using sensorless current-based model predictive control.' IEEE Trans. Ind. Appl. 53(2), 1157–1167 (2016)
36. Shadmand, M.B., Mosa, M., Balog, R.S., Rub, H.A.: An improved mppt technique for high gain dc-dc converter using model predictive control for photovoltaic applications. In: IEEE Applied Power Electronics Conf. and Exposition-APEC 2014, pp. 2993–2999. IEEE, Piscataway (2014)

How to cite this article: Priyadarshi, N., Sanjeevikumar, P., Bhaskar, M.S., Azam, F., Muyeen, S.M.: An improved standalone photovoltaic system with hybrid dual integral sliding mode and model predictive control for MPPT. IET Renew. Power Gener. 1–15 (2022). https://doi.org/10.1049/rpg2.12665